Nov 7th, 12:00 AM - Nov 8th, 12:00 AM

Low Fatigue Response of Crest-Fixed Cold-Formed Steel Drape Curved Roof Claddings

Krishanu Roy

James B. P. Lim

Amir Mohammad Yousefi

G. Charles Clifton

Mahen Mahendran

Wei-Wen Yu International Specialty Conference on Cold-Formed Steel Structures
St. Louis, Missouri, U.S.A., November 7 & 8, 2018

Low fatigue response of crest-fixed cold-formed steel drape curved roof claddings

Krishanu Roy[1a], James B.P. Lim[1b], Amir Mohammad Yousefi[1c], G Charles Clifton[1d], Mahen Mahendran [2e]

[a] PhD student, Email: kroy405@aucklanduni.ac.nz

[b] Associate Professor, E-mail: james.lim@auckland.ac.nz

[c] PhD student, Email: ayou561@aucklanduni.ac.nz

[d] Associate Professor, E-mail: c.clifton@auckland.ac.nz

[e] Professor, E-mail: m.mahendran@qut.edu.au

Abstract

Cold-formed steel roof claddings are subjected to significant suction/uplift pressures during high wind events. In New Zealand, the strong prevailing winds makes this a common occurrence. Suction pressures are generated by the turbulence of the wind flow around the building which can vary both spatially and temporally. The weakest link in the roofing system is the connection between roof sheeting and screw fasteners, which if fails, can lead to progressive collapse of the whole roofing assembly. Fluctuating high wind suction pressures can result in either static or fatigue pull-through failure of the roof sheeting at its screw fastener connections. Current literature has covered the static and fatigue wind uplift performance of crest-fixed corrugated and trapezoidal roof claddings. However, no research has been undertaken to understand the wind uplift performance of the typical crest-fixed cold-formed steel drape curved roof claddings used in New Zealand. This issue is addressed herein. In total, 35 large scale experimental tests are presented for crest-fixed drape curved steel roof claddings subjected to static and cyclic wind suction/uplift loads applied using a Pressure Loading Actuator. The material properties of claddings were determined using tensile coupon tests while the initial geometric imperfections of claddings were measured using a laser scanner. The critical fastener reactions were determined using a three axis load cell. Crack initiation, propagation of cracks, crack patterns and the number of load cycles to failure are discussed for such claddings under different load levels. Tests showed that the drape curved roof claddings are also subjected to localised dimpling and pull-through failures at their screw connections under static and cyclic wind uplift loads with the occurrence of low cycle fatigue failures under cyclic loading.

Keywords: Cold-formed steel, Drape curved roof, Roof claddings, Fatigue, Crest-fixed, Fastener

1 Introduction

Cold-formed, thin steel roof and wall claddings are commonly used in low-rise residential and commercial buildings because of their superior strength to self-weight ratio, higher span capacity, good durability, high resilience in earthquakes and ease of construction. These steel claddings are mostly fastened to the purlins/battens at their crests with screw fasteners. In such an arrangement, crest-fixed steel claddings suffer from either local dimpling failure and/or pull-though failures at the screw fastener holes when subjected to wind uplift/suction pressures during high wind events [1]. Pull-through failures are initiated by transverse splitting/fracture or low cycle fatigue cracking at the fastener holes, which lead to disengagement of roof sheeting. Therefore, wind-uplift/suction capacity of crest-fixed steel claddings is governed by localised pull-through failures at the screw connections.

In the literature, significant research has been described for crest-fixed corrugated and trapezoidal steel claddings under wind-uplift/suction pressures to understand the failure mechanisms of such claddings [2-5]. Mahendran [2-3] investigated the static and fatigue behavior of crest-fixed corrugated roofing under simulated cyclonic wind loading. Xu [4] considered both corrugated and trapezoidal profiles in investigating the fatigue performance of crest-fixed light gauge steel claddings under fluctuating wind uplift loading.

To extend this work, Mahendran [5] studied the fatigue loading sequence for roof claddings in cyclone prone areas and developed a simplified loading matrix. Similar investigations were also carried out by Kumar and Stathopoulos [6] and Kumar [7] to study the fatigue performance of roof cladding under simulated wind loading. All these investigations were based on expensive laboratory tests. However, Jancauskas et al. [8] presented an analytical model to simulate the fatigue behavior of roof cladding during the passage of a tropical cyclone. On the other hand, Mahaarachchi and Mahendran [9-10] developed a shell finite element model which can predict the pull-through failure of crest-fixed trapezoidal steel claddings. The finite element model included an appropriate splitting criteria for trapezoidal claddings, which was developed by Mahaarachchi and Mahendran [11]. Henderson and Ginger [12] studied the low-cycle fatigue response of corrugated metal roof cladding by using more realistic application of static, cyclic and simulated wind loads. In their research, they characterized the different crack patterns of crest-fixed corrugated roof claddings. Lovisa et al. [13] extended this work by performing an experimental investigation into the fatigue behavior of corrugated cladding and quantitatively characterized the crack initiation using a strain criterion. However, it is worth mentioning that all these investigations were either for the conventional corrugated or for trapezoidal steel claddings.

In New-Zealand and neighbouring countries, the crest-fixed drape curved roofs (see Fig.1) are increasingly being used in low-rise buildings. No research has been undertaken on this roofing profile under wind uplift loading. Also, there are no adequate design guidelines available, for drape curved roofs under wind uplift loading. Eurocode [14] and American Iron and Steel Institute (AISI) [15] include design recommendations for valley fixed drape curved roofs made with thicker (>0.6 mm) and softer (yield stress <450 MPa) materials, which may not be applicable to New-Zealand's drape curved roofs which are made of thin, high strength steels and are crest-fixed.

In this research, large scale experiments were conducted on drape curved claddings, subjected to two types of loading: (a) Static wind uplift pressure and (b) Cyclic wind uplift pressure. Although the wind uplift pressure on roof cladding fluctuates randomly in space and time during high wind events, in the experimental tests it is difficult to simulate higher wind pressure along the edge of the roof, therefore a static uniform wind-uplift/suction pressure and a constant amplitude cyclic wind uplift/suction pressure were used in this study. More than 30 large scale experimental tests were conducted and the results are reported herein. The important fastener reactions were measured by using a 3-axis load cell. Local dimpling, transverse splitting, crack initiation, propagation of cracks and crack types are discussed in detail for such claddings under different load levels. Material properties of the claddings were determined using tensile coupon tests while initial geometric imperfections were measured using a laser scanner. This paper presents the details of this experimental investigation on the drape curved steel claddings subject to static and cyclic wind uplift/suction pressure loading and the results.

2 Experimental investigation

2.1 Cladding specimens

The drape curved roof/wall claddings were rolled from a G550 coil, which refers to the specified minimum yield strength of 550 MPa. Two different base metal thicknesses (BMT) were considered: 0.40 mm and 0.55 mm. Fig. 2 shows the cross-sections of the cold-formed steel drape curved claddings considered in this research. Three sheets were used in the experimental tests to consider the overlap between two cladding sheets.

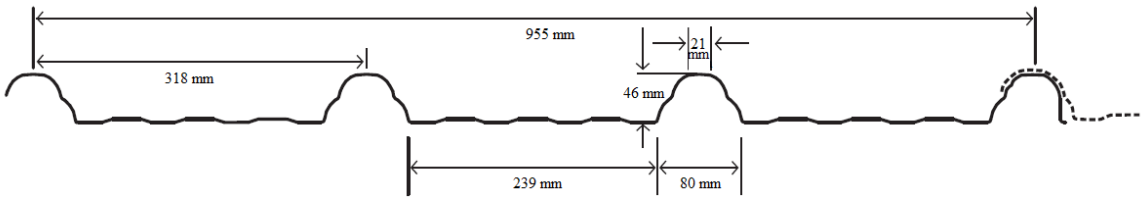

Figure 1: Nominal cross-sections of cold-formed steel drape curved claddings considered in this paper

2.2 Cladding fixings

The claddings were fixed to battens/purlins at different spacing, varying from 500 to 2000 mm as shown in Fig. 2. They were attached to the batten or purlin using either self-drilling timber or metal screws (screw head diameter of 14 mm) depending on the type of support. No 14-10×65 mm Type 17 self-drilling screws with EPDM washers were used for cladding fixings. The cladding screws had a weather sealed washer, which is

approximately12 mm in diameter. Claddings were fixed by self-drilling screws at the middle of each crest and set perpendicular to the plane of the sheet. All the screws were tightened using a torque controlled screw gun to the manufacturer's recommended installed torque to avoid over-tightened or loose screws.

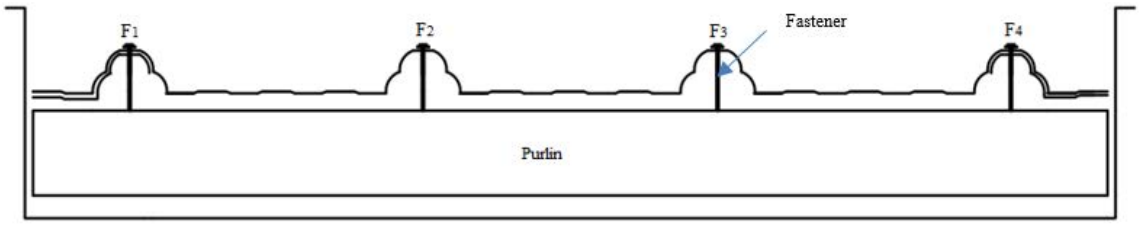

(a) Elevation

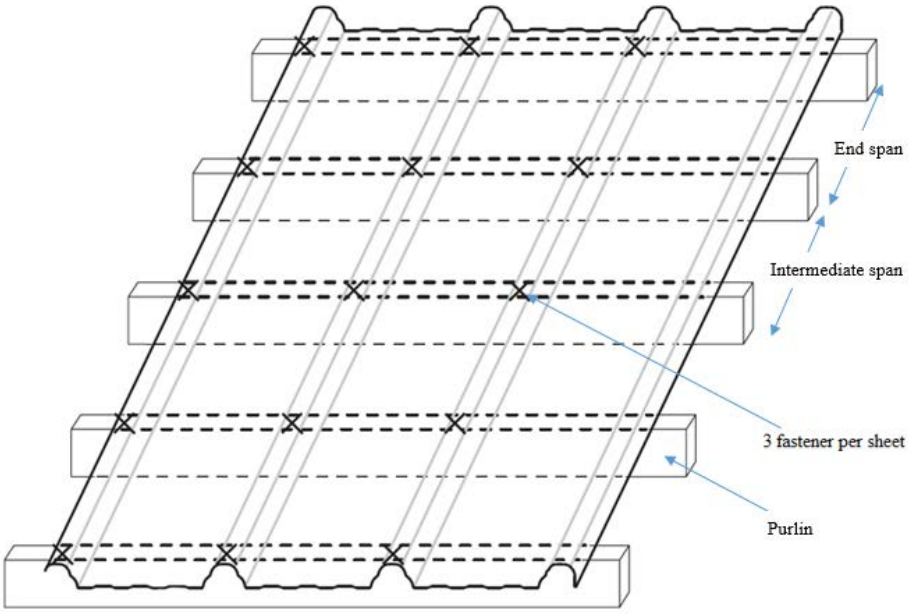

(b) Plan view

Figure 2: Cladding fixings

2.3 Specimen labelling

The crest-fixed cold-formed steel drape curved claddings were labelled such that the type of cladding assembly, cladding span and thickness were expressed by the label. For example, the label "DCR- S600 -t0.55 is explained as follows:

- "DCR" indicates the type of cladding profile, which is drape curved roof.
- "S600" represents the cladding span of 600 mm, i.e. the spacing between adjacent purlins/battens.
- "t0.55" represents the nominal thickness of the cladding profile of 0.55 mm.

2.4 Cladding material properties

In order to determine the material properties of cladding specimens, tensile coupon tests were conducted. The tensile coupons were prepared from the centre of the cladding sheets tested herein, in accordance with ISO 6892-1:2009 [16]. Five coupons were obtained from both longitudinal and transverse directions of the cladding sheets. The coupons were tested in an Instron 4469 tensile testing machine which has a capacity of 50 kN. A calibrated extensometer of 50 mm gauge length was used to determine the tensile strain of the coupons. The average Young's modulus and yield strength from these tests were 205 GPa and 568 MPa, respectively for 0.40 mm thick profile claddings, whereas for 0.55 mm thick claddings, Young's modulus and yield strength were 201 GPa and 557 MPa, respectively.

2.5 Test-rig and testing procedure

Simply supported crest-fixed drape curved roof claddings were tested under static and cyclic wind-uplift pressures in a rectangular pressure box of dimensions 5000 mm×2000 mm×320 mm. Four-span roofing assemblies were tested as shown in Fig. 3. The end spans were taken as two-thirds of the intermediate span according to the manufacturer's recommendation. A vacuum pump and pressure loading actuator (PLA) was

used to simulate the required wind pressure inside the pressure box. Polystyrene foam was used to fill the gaps on both side of drape curved steel cladding assembly to stop any leakage of air.

Pull-through or local-dimpling failure is the most common failure mode [10] of such claddings when subjected to wind uplift pressure, which is controlled by the load per screws at the central and edge supports. Therefore, two 5 kN S-type load cells and one 15 kN 3-axis load cell (see Fig. 4) were used to determine the screw fastener loads at three of the central support screws. Eight LVDTs were used to measure the deflections at central support and mid-pan. LVDT positions are shown in Fig. 4. Three pressure sensors of each 20 kPa capacity were used measure the uniform pressure inside the pressure box. As shown in Fig. 3, four mounting frames were used to place the LVDTs and load cells on top of the cladding sheets. It is expected that wind uplift pressure will cause large longitudinal and transverse strains around the screw fastener holes. Therefore, four strain gauges (gauge length of 2 mm), one on each side of the fastener hole, were used to measure the longitudinal and transverse strains of three critical central support screws (see Fig. 4(d)). As the wind pressure is increased, the large stress concentration will cause dimpling failure initially around the fastener holes, which will lead to pull-through failure finally under increasing uplift pressure.

Figure 3: Photograph of the pressure box

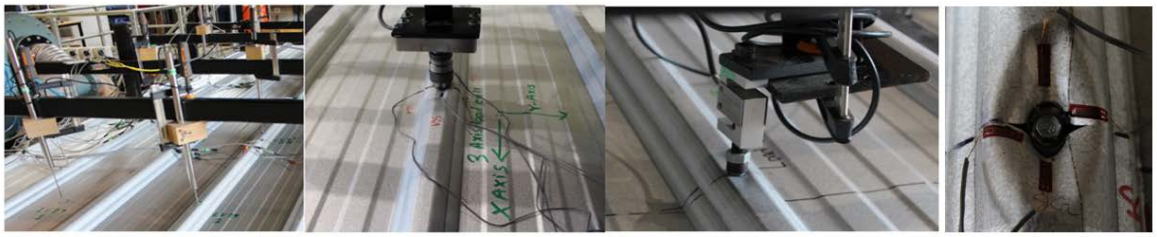

(a) LVDTs (b) 3-Axis load cell (c) S-type load cell (d) Strain gauges

Figure 4: Locations of sensors

2.6 Measurement of initial geometric imperfections

Fig. 5 shows the details of the laser scanner assembly used to measure the initial geometric imperfections present in the drape curved claddings. As can be seen in Fig. 5, it is comprised of a 5500 x 2500 x 1500 mm steel frame which supports a travelling platform mounted on precision rails in the longitudinal (5500 mm) direction. The platform supports a stepper motor (see Fig. 5(a)), which allows displacement controlled motion using a rack and pinion system. The platform is designed to have a precision shaft in the transverse (2500 mm) direction which guides a moveable laser scanner. The laser scanner records reading at every 0.0001 mm along each of the mid-crest and mid-pan of the cladding profiles. A typical plot of the initial geometric imperfections versus length is shown in Fig. 5(c). The maximum initial imperfections of the cladding specimens are shown in Table 1.

(a) Stepper motor (b) Laser scanner assembly

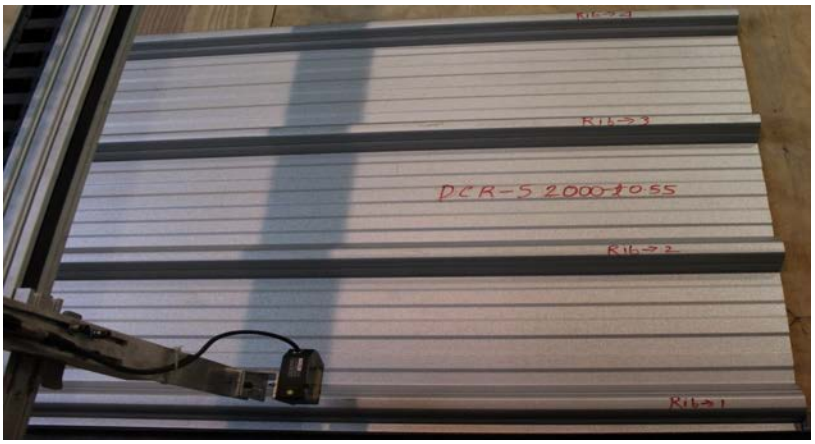

(b) Photograph of imperfection measuring setup

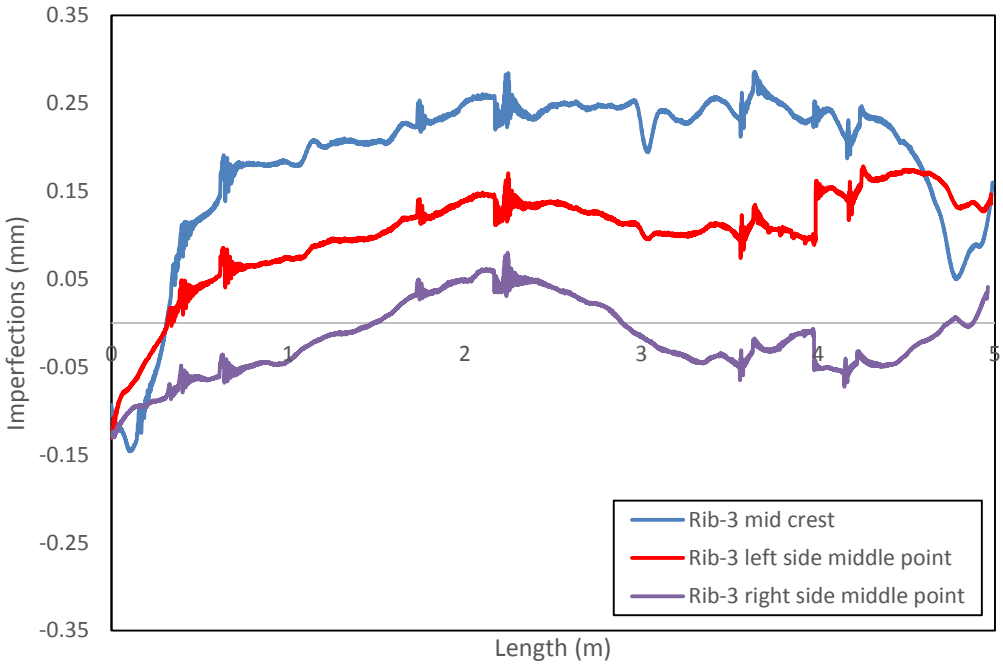

(c) Typical imperfection profile (DCR-S2000-t0.55)

Figure 5: Measurement of initial geometric imperfections using a laser scanner

Table 1: Measured initial geometric imperfections

Specimen	Maximum imperfections (mm)
DCR-S500-t0.55	0.28
DCR-S800-t0.55	0.16
DCR-S1200-t0.55	0.29
DCR-S1500-t0.55	0.22
DCR-S2000-t0.55	0.09
DCR-S500-t0.40	0.14
DCR-S800-t0.40	0.18
DCR-S1200-t0.40	0.16
DCR-S1500-t0.40	0.22
DCR-S2000-t0.40	0.24

2.7 Loading procedure

The drape curved steel claddings were loaded under two types of wind pressures as described below:

2.7.1 Static wind uplift pressure

All test specimens were loaded under a steadily increasing, spatially-uniform uplift pressure as shown in Fig. 6(a). The uplift pressure was increased by 2 kPa after stabilizing the pressure for 30 seconds each time. Initially, the cladding deflection increased linearly with uplift pressure up to a pressure of 1.43 kPa. Local deformation of cladding near the screw head was observed during that period. As the pressure was increased beyond 1.43 kPa, non-linear behaviour was observed; i.e. the deflection of cladding increased non-linearly with wind-uplift pressure because of the localised dimpling of the cladding under the screw head.

2.7.2 Cyclic wind uplift pressure

Cyclic tests were conducted by means of applying sinusoidal loads to the test specimens (see Fig. 6(b)) The sinusoidal pressures were applied at a frequency of 1.2 Hz. The fatigue behaviour of the drape curved steel claddings was studied in terms of the number of cycles to failure, fastener reactions, crack initiation, crack propagation and different types of crack patterns. Cyclic uplift pressure loading applied to the drape curved steel claddings until fatigue failure occurred with the cladding pulling over/through at least one of the screws as per AS/NZS 1170.2 [17].

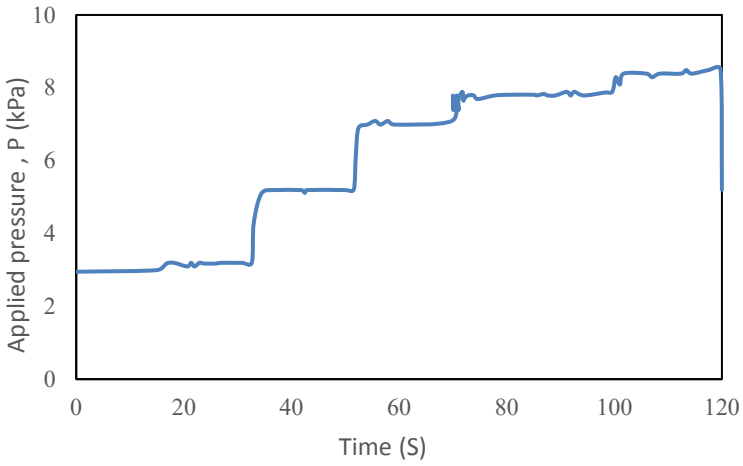

(a) Static uplift pressure applied in steps (DCR-S1200-t0.55)

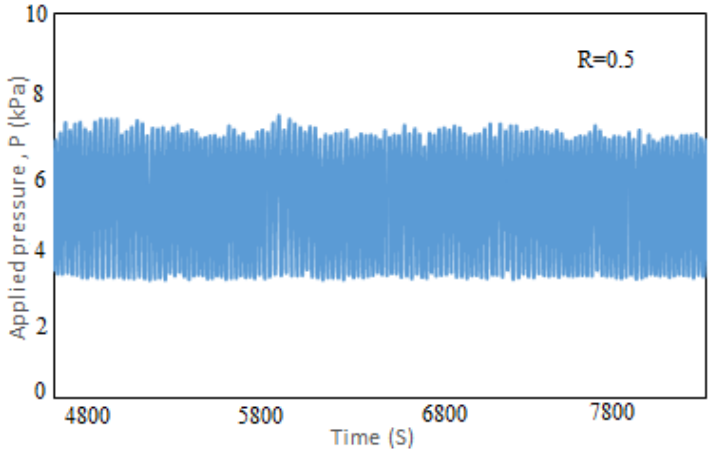

(b) Cyclic uplift pressure (DCR-S500-t0.55)

Figure 6: Static and cyclic uplift pressures applied to the drape curved steel claddings

2.8 Experimental results

Experimental results are discussed separately for static and cyclic wind uplift pressures as shown next.

2.8.1 Cladding response under static wind uplift pressure

Fig. 7 shows the deflected shape of the DCR-S2000-t0.55 under static wind-uplift pressure. The load in the screw fastener along the Z-axis is given by the equation below:

$$F_Z = C_R \times P \times A \quad (1)$$

where C_R is the reaction coefficient, P is the uniform uplift pressure and A is the tributary area of the fastener (i.e., cladding span ×fastener spacing). For a two-span wind load test, the value of C_R is recommended in between 1.15 to 1.25 from previous research [1]. The value of C_R depends on the level of loading and the cladding profile. For these four-span tests, an average C_R value of 1.11 provided the best agreement between the experimental fastener load and the fastener load calculated from equation-1 (see Table 2).

The deflected shape of the DCR-S2000-t0.40, subjected to wind uplift pressure is shown in Fig. 7. The screw fastener loads, F_X, F_Y and F_Z in x, y and z directions were measured by the 3-axis load cell at the fastener F_3 (see Fig. 2a) for a stepped static applied pressure and the results are shown in Fig. 8. As can be seen from Fig. 8, first spike in F_X, F_Y and F_Z happened at 44.8 seconds when the cladding adjacent to the fastener dimpled. The lateral load (F_X) on the "fastener" is approximately 8% of F_Z. Another spike is seen in F_X, F_Y and F_Z values at 75 seconds when the cladding profile starts splitting transversely at the fastener hole. This reduces the stiffness of the cladding profile and hence reduces the reaction coefficient. During the fourth load step, the cladding splits completely at the fastener hole. Pull-through failure loads as fastener loads and wind uplift pressures are shown in Table 2 for all cladding specimens tested under static uplift wind pressures.

Figure 7: Deflected shape of the drape curved roof cladding (DCR-S800-t0.55)

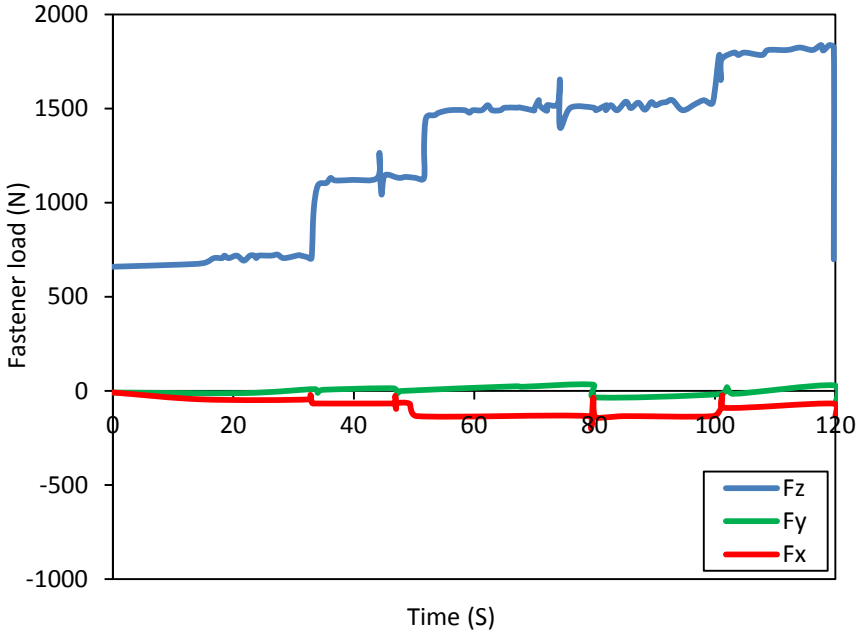

Figure 8: Loads in the critical fastener F_3 of central support under static step pressure loading

Table 2: Fastener loads at failure under static wind-uplift pressure

Specimen	Span (S) (mm)	Thickness (t) (mm)	Failure pressure (P) (kPa)	Experimental fastener load, $F_{Z\text{-}EXP}$ (N)	Design fastener load from eq-1, $F_{Z\text{-}eq\text{-}1}$ (N)	Comparison $F_{Z\text{-}EXP}$ / $F_{Z\text{-}eq\text{-}1}$ -
DCR-S500-t0.55	500	0.55	12.36	2795.8	2662.7	1.05
DCR-S800-t0.55	800	0.55	10.14	2710.4	2657.3	1.02
DCR-S1200-t0.55	1200	0.55	8.45	2547.6	2449.6	1.04
DCR-S1500-t0.55	1500	0.55	7.46	2415.4	2322.5	1.04
DCR-S2000-t0.55	2000	0.55	6.24	2335.7	2224.5	1.05
DCR-S500-t0.40	500	0.40	10.21	2434.8	2297.0	1.06
DCR-S800-t0.40	800	0.40	8.57	2348.7	2236.9	1.05
DCR-S1200-t0.40	1200	0.40	7.28	2194.7	2070.5	1.06
DCR-S1500-t0.40	1500	0.40	6.23	2078.9	1979.9	1.05
DCR-S2000-t0.40	2000	0.40	5.16	1824.6	1721.3	1.06

As shown by Table 2 results, the wind uplift pressures and the critical screw fastener loads at failure reduce with increasing span, although the differences are small for shorter spans in the range of 500 to 1200 mm. When the cladding thickness was reduced from 0.55 to 0.40 mm, the reduction in failure load/pressure was small for shorter spans, but increased significantly for long spans by about 40%.

2.8.2 Cladding response under cyclic wind uplift pressure

Cladding response was observed under the cyclic wind uplift pressure loading applied to the specimens and the number of cycles to failure was recorded. The corresponding fastener loads, F_X, F_Y and F_Z under the applied cyclic wind uplift pressure, are shown in Fig. 9. As can be seen, a spike in F_X and F_Y at about 35.6 seconds, indicates the local dimpling failure of the cladding in the vicinity of the fastener holes. The dimpling of the claddings at the screwed crests transfers a lateral load (F_X and F_Y) to the screws, typically in the order of 50 to 200 N. When the number of cycles is increased, local dimpling of cladding initiates the pull-through failure by means of transverse splitting of the cladding at the fastener holes.

Cold-formed steel roof claddings are susceptible to low-cycle fatigue failure. Low-cycle fatigue is generally known as the failure within 10,000 load cycles [18]. Cladding failure may occur either from a large number of low pressure load cycles or from a low number of high wind pressure cycles.

Cyclic tests were carried out at a similar peak load as static wind uplift tests but with different *R* values of 0.1 to 0.5. *R* is the load ratio, defined as $R=S_{min}/S_{max}$, where, S_{max} is the maximum load and S_{min} is the minimum load applied during the tests. About five cyclic tests were conducted for each load ratio, giving a total of 25 cyclic tests. The maximum wind uplift pressures applied in each test can be seen in Fig. 10. Five different spans were tested for each load ratio. Only 0.55 mm thick claddings were tested under cyclic loading (see Table 3). From the experiments, it was observed that the cyclic failure pressure was approximately 70% of the static failure pressures on average for all tests. The number of load cycles to failure is dependent on the load ratio (*R*). Fig. 10 shows the maximum cyclic uplift pressures (P_{max}) versus the number of cycles to failure (N_i) for different values of load ratios (*R*).

Table 3: Maximum uplift pressure applied at failure during cyclic tests

	Maximum uplift pressure (kPa)				
Specimen	Load Ratio (*R*= 0.1)	Load Ratio (*R*= 0.2)	Load Ratio (*R*= 0.3)	Load Ratio (*R*= 0.4)	Load Ratio (*R*= 0.5)
DCR-S500-t0.55	4.53	5.23	6.01	6.84	7.36
DCR-S800-t0.55	4.23	4.88	5.09	5.46	6.89
DCR-S1200-t0.55	3.81	4.06	4.31	4.89	6.23
DCR-S1500-t0.55	3.21	3.61	3.87	4.08	5.42
DCR-S2000-t0.55	2.58	2.91	3.25	3.64	4.28

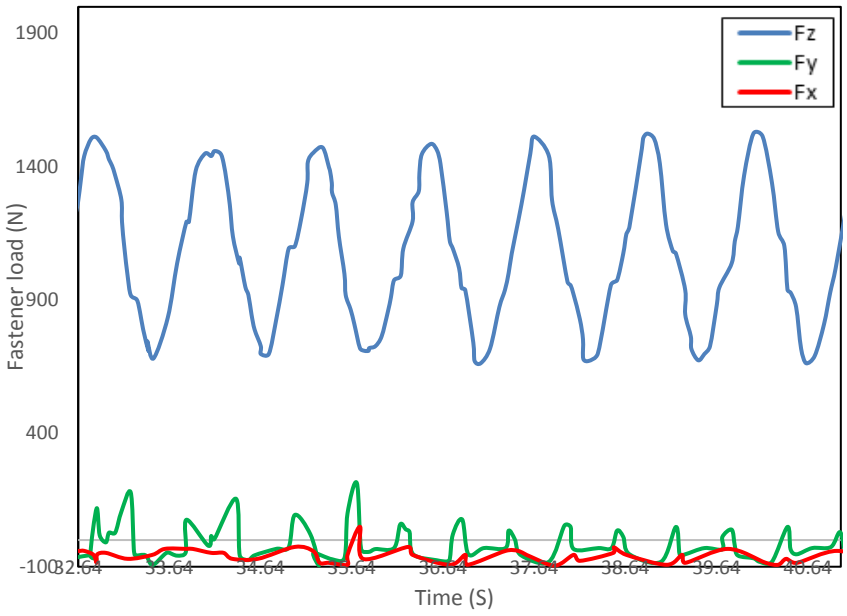

Figure 9: Loads in the critical fastener F_3 of central support under cyclic wind pressure loading

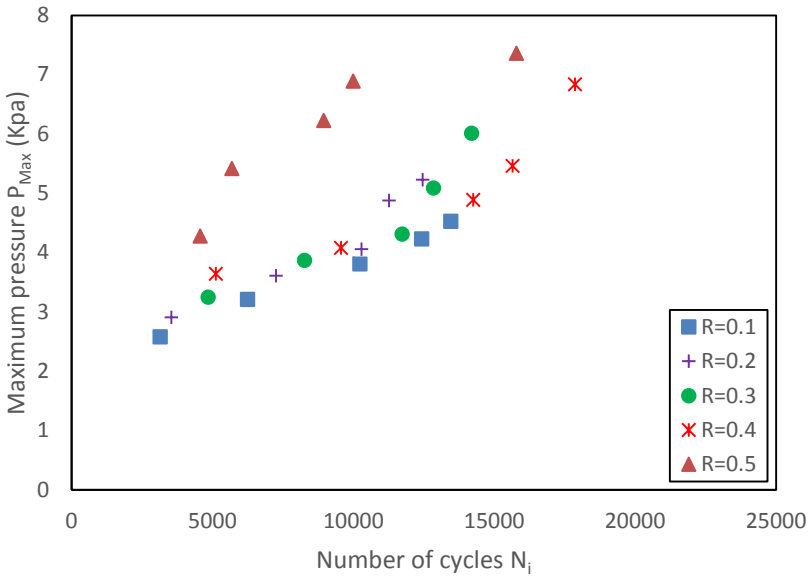

Figure 10: Maximum cyclic wind pressure versus the numbers of cycles to failure for varying R values

As shown in Fig. 10, roof cladding suffered low cycle fatigue failures at lower load ratios of 0.1 and 0.2, i.e. the number of cycles to failure was less than 10000. However, as expected with increasing load ratios (0.5), the number of cycles to failure increased to about 18,000 even with higher maximum wind uplift pressure.

3. Types of Failure

The static and cyclic wind uplift loading produced different types of failure patterns in drape curved claddings. Failure patterns from both static and cyclic tests are discussed separately in the following sections:

3.1.Static wind uplift pressure loading

Drape curved roof claddings were subjected to static wind uplift pressure until the failure in terms of either local dimpling or transverse splitting occurred around the fastener holes. Drape curved roof failure modes under static wind uplift pressures are discussed below.

3.1.1 Dimpling failure

Dimples were formed near the edges of the deformed crests in the cladding profile at a pressure greater than 3 kPa, however complete dimpling failure was observed at uplift pressure greater than 5kPa. As the wind pressure was increased, longitudinal and transverse bending actions near the fastener hole were observed, leading to the large cross-sectional deformation of the drape curved steel claddings. These cross-sectional deformation results in large stress concentrations around the fastener holes leading to the local dimpling failure of cladding profile. Most of the dimpling failures occurred at uplift pressure less than 6.24 kPa for static tests. Dimpling failure of a drape curved roof under static wind-uplift loading is shown in Fig. 11(a).

3.1.2 Initiation of transverse splitting along with dimpling failure

When the local dimpling displacement goes beyond 5 mm [19], the transverse splitting starts at the fastener hole. This is mainly a transition phase between the dimpling failure and splitting failure (see Fig. 11(b)), when the non-linear behaviour starts with increase in wind-pressure. This failure occurred in static tests at a pressure higher than 6.24 kPa. A second spike in F_Z, F_Y and F_X was observed at 74 second, when the transverse splitting initiated at the drape curved claddings around the fastener holes (see Fig. 8).

3.1.3 Transverse splitting failure

When the wind pressure was increased beyond 6.24 kPa , the cladding profile started splitting in Y directions around the fastener hole (see Fig. 11(c)). As a result of this, the fastener load in Y direction (F_Y) increased by around 36%. However, no longitudinal splitting was observed, the drape curved roofs did only split in the transverse direction (Y-direction), this is because of the discontinuity of the crest in the transverse direction. The transverse strains were recorded from the strain gauges installed near the fastener holes to develop a suitable strain criterion for drape curved steel claddings under static wind-uplift pressure (see Fig. 11(c)).

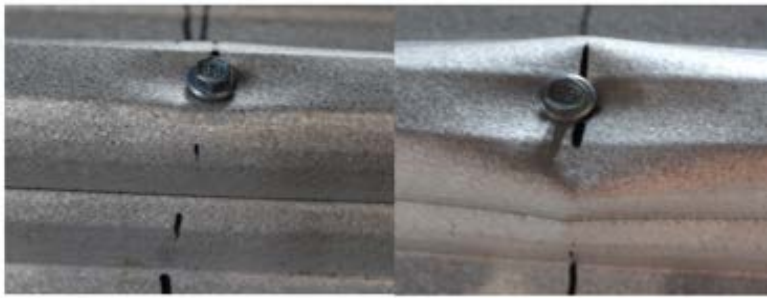

(a) Dimpling failure

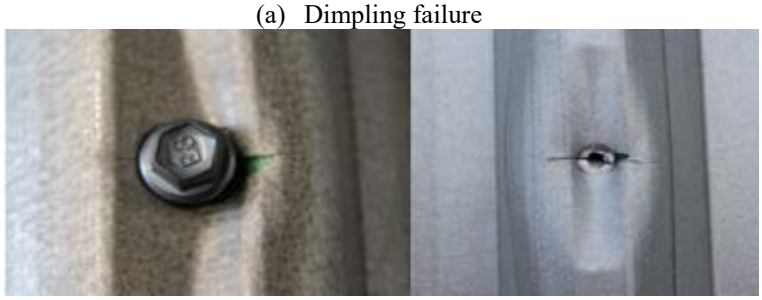

(b) Initiation of transverse splitting following dimpling

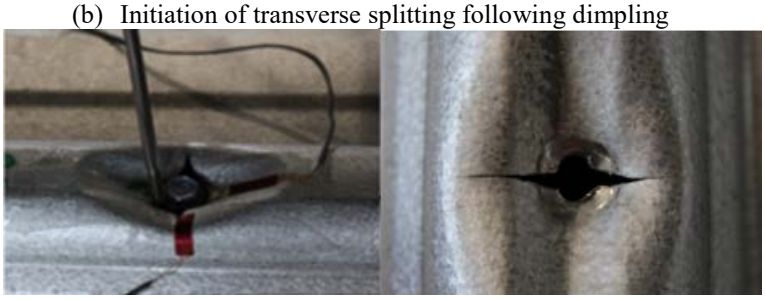

(c) Transverse splitting failure

Figure 11: Different types of failures in drape curved claddings under static uplift loading

3.2 Fatigue failure

Fatigue failure starts with dimpling and splitting failure which is the same failure pattern as observed in static tests. However, at higher loads, different crack patterns were observed in cyclic tests. A crack initiates, if the length of the crack is more than 1 mm in either direction (X or Y). The numbers of load cycles for crack initiation and for ultimate failure may not necessarily be for the same fastener in the cladding . It is expressed as the threshold numbers of load cycles for crack initiation and ultimate failure of any one of the four fasteners i.e. F_1-F_4, as shown in Fig. 2(a) in each test. Fig. 13 characterizes the number of load cycles at which different types of failures are initiated and the maximum pressure at failure is recorded. The different types of failures in cyclic tests are discussed below:

3.2.1 Dimpling failure

For cyclic tests, dimpling failure (see Fig. 13) occurred at number of load-cycles less than 3500 and at a minimum pressure of 2.58 kPa. Fig. 12(a) shows the picture of dimpling failure occurred in cyclic tests for DCR-S2000-t0.55. Cladding deflection was linear up to a wind pressure of 1.6 kPa, after which non-linear behaviour was observed i.e. the longitudinal and transverse bending was observed near the fastener hole. The bending action resulted in large cross sectional deformation around the fastener holes, when the wind pressure was increased up to 2.58 kPa, leading to the dimpling failure of cladding profile.

3.2.2 Splitting failure

When the wind load was increased beyond 5.42 kPa for cyclic tests, the cladding profile started splitting in both X and Y directions around the fastener hole (see Fig. 12(b)). As a result of this, the fastener load in X direction (F_X) increased by around 16%. The longitudinal and transverse strains were recorded from the strain gauges installed near the fastener holes to develop a suitable strain criteria for drape curved steel claddings (see Fig. 12(c)). Two dimensional splitting of drape curved steel claddings occurred at load cycles in the range of 5500 to 10000, as shown in Fig. 13. As expected, splitting failure was observed for DCR-S800-t0.55, DCR-S1200-t0.55 and DCR-S1500-t0.55 at the highest load ratio (0.5).

3.2.3 T-type cracks

T-type cracks were initiated near the screw head of the fastener in the cladding profile under sinusoidal loading (cyclic loading). T-type cracks are shown in Fig. 12(c). X and Y fastener loads i.e. F_X and F_Y varies linearly up to 3.5 kPa, after which non-linear behaviour was observed until T-type cracks were formed. T-type cracks were formed in between the load-cycles of 4500 and 8,200 for DCR-S1500-t0.55 and DCR-S2000-t0.55

The load ratio (R) was in the range of 0.1 to 0.3 for DCR-S1500-t0.55, while for DCR-S1500-t0.55, the load ratio (R) was from 0.3 to 0.5. From the strain gauge readings, it was observed that, the strain values were increased linearly up to a pressure of 3.5 kPa, after which longitudinal strain values increases in a much faster rate than transverse strain around the fastener hole, leading to pulling over of drape curved steel cladding in the form of T-type cracks. T-type cracks were formed in a pressure range of 3.87 to 4.28 kPa.

3.2.4 Star-type cracks

Star-type cracks were formed in the drape curved steel claddings under cyclic loading, at the screw hole as shown in Fig. 12 (d). Star-type cracks formed at higher pressure than T-type cracks (in between 4 to 5 kPa). Longitudinal and transverse strain values were measured with the help of strain gauges, which were installed in the cladding, near the screw head (see Fig. 12(d)). Most of the star-type cracks were formed at number of load cycles in between 10000 to14000 for DCR-S500-t0.55, DCR-S800-t0.55 and DCR-S1200-t0.55, when the load ratios (R) were in the range of 0.1 to 0.3.

3.2.5 O-type cracks

O-type cracks were observed in the cladding near the vicinity of screw head under cyclic loading. O-cracks were formed at much higher wind-uplift pressure than for star-type crack patterns i.e. in the range of 4.46 kPa to 7.36 kPa (see Fig. 13). Number of load cycles were also the highest (from 14000 to 17000) for O- type cracks to be formed. DCR-S500-t0.55 and DCR-S800-t0.55 showed this type of cracks during cyclic tests. For, DCR-S500-t0.55, load ratio (R) was in range of 0.3 to 0.5 (maximum), while for DCR-S500-t0.55, O-type crack was observed at load ratio (R) of 0.4. The lateral loads F_X and F_Y increased linearly with pressure and increasing number of load-cycles until the O-type crack was formed (see Fig. 12(e)). However, non-linear variation of X and Y fastener loads were observed during the growth of crack as number of load cycles go past 14225.

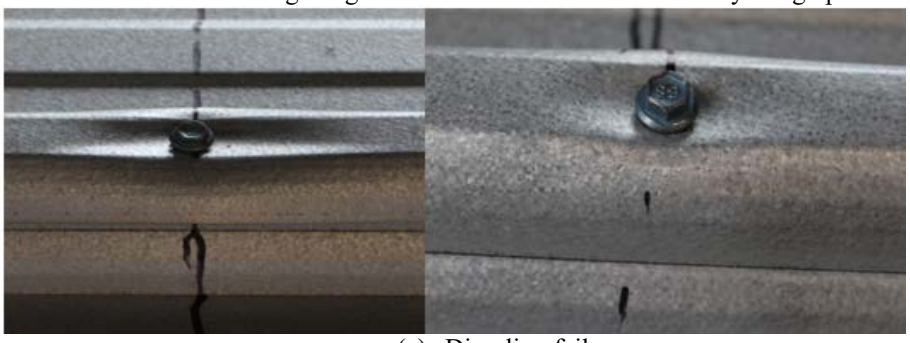

(a) Dimpling failure

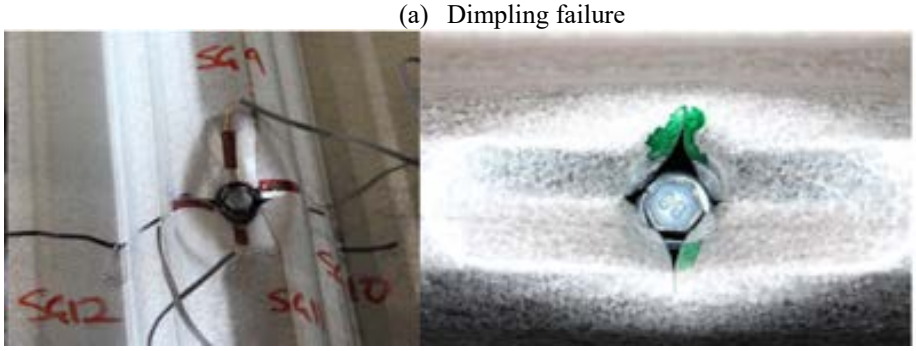

(b) Splitting failure

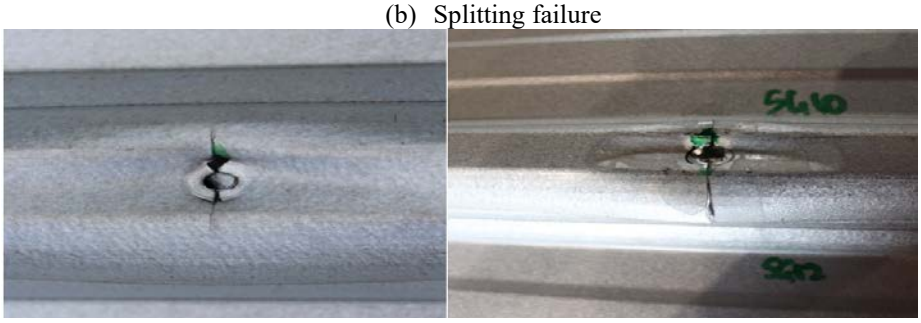

(c) T-type crack

(d) Star-type crack

(e) O-type crack

Figure 12: Different types of failures and cracks patterns in drape curved claddings under and cyclic loading

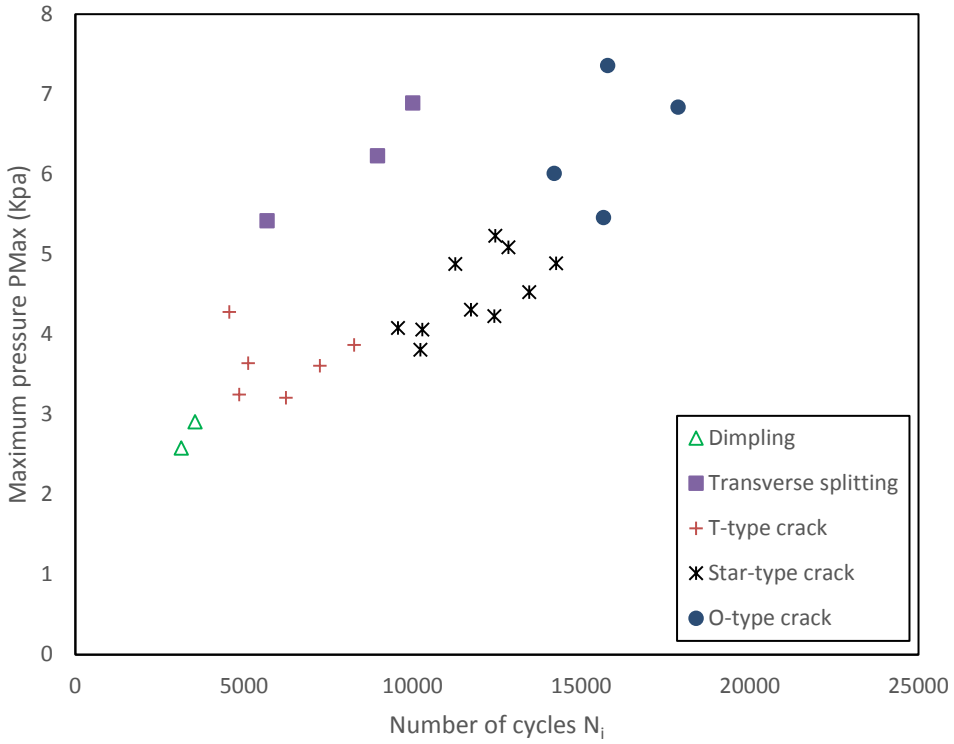

Figure 13: Maximum uplift pressure versus the number of load cycles for different types of failure patterns in cyclic tests

4. Conclusions

This paper has presented the details of an experimental investigation into the pull-through failure mechanisms of crest-fixed drape curved cold-formed steel claddings, commonly used in New-Zealand, under wind uplift/suction pressure loading. The results from more than 30 full scale pressure-box tests on drape curved cladding profiles have been used to characterize the localised pull-through failures under both static and cyclic wind uplift pressure loading. The material properties of the claddings were determined using tensile coupon tests while their initial geometric imperfections were measured using a laser scanner. The imperfection values would be used in the finite element model to be developed for such claddings under wind uplift loads. The paper also

discusses the static and fatigue behaviour of drape curved cladding assemblies in terms of localised dimpling, transverse splitting, crack initiation and different types of cracks at failure. The results reported in this paper show that the crest-fixed drape curved steel cladding assemblies are also subjected to localised dimpling and/or cracking around the screw fastener holes leading to pull-through failures under wind uplift loading. Unlike corrugated and trapezoidal profiles, drape curved claddings showed T- and O-type cracks under cyclic loading.

The screw fastener reaction at the critical supports were determined using 3-axis load cells and it was found that the lateral loads are also important along with the vertical uplift loads as they contributed to the different failure patterns, i.e. dimpling, transverse splitting, non-uniform crack growth. The critical central fastener loads could not be predicted accurately using the simple engineering formulae available in the literature unless appropriate modifications are made to the reaction coefficient. With suitable modification to the reaction coefficient, the design equation is only 5% conservative with respect to the experimental results.

5. Future work

The first author is currently developing a numerical model to investigate the different parameters affecting the pull-through failure of drape curved cold-formed steel claddings subjected to static and cyclic wind uplift loads. A second focus is to consider the effect of fluctuating cyclic wind uplift loading as generated by actual winds. It is important to determine the influence of fluctuating wind loading on the pull-through mechanism of drape curved claddings. A splitting criterion is to be developed to include in the numerical models. Ongoing work will aim to develop better design methods for drape curved roof cladding used in New Zealand.

Acknowledgments

The experiments were conducted in the University of Auckland, New-Zealand. Authors would like to acknowledge the support of Mr. Lee, Garett Webb, Mike Edwards, Matthew Muir and Lance Inglis from the KS Holdings Ltd. and the The Roofing Store Ltd., New-Zealand for providing specimens and test-rig facilities. Also, the continuous support of John Bisschops from The Roofing Store Ltd. is greatly acknowledged.

References

[1] Mahendran M. Behaviour and design of crest-fixed profiled steel roof claddings under wind uplift. Eng Struct 1994; 16: 368–76.

[2] Mahendran M. Fatigue behaviour of corrugated roofing under cyclic wind loading. Civil Engineering Transactions IE Aust; 1990.

[3] Mahendran M. Fatigue behaviour of corrugated roofing under cyclic wind loading. Cyclone testing station technical report 35. Townsville: James Cook University, JCU; 1989.

[4] Xu YL. Fatigue performance of screw-fastened light-gauge-steel roofing sheets. J Struct Eng ASCE 1995; 121: 389–98.

[5] Mahendran M. Towards an appropriate fatigue loading sequence for roof claddings in cyclone prone areas. Eng Struct 1995; 17: 476–84.

[6] Kumar S, Stathopoulos T. Fatigue analysis of roof cladding under simulated wind loading. J.Wind Eng(Ind.Aerodyn) 1998; 77(8): 171-183.

[7] Kumar S. Prediction of wind-induced fatigue on claddings of low buildings. Computers and Structures 2000; 75 (1): 31–44.

[8] Jancauskas E, Mahendran M, Walker G. Computer simulation of the fatigue behaviour of roof cladding during the passage of a tropical cyclone. J.Wind Eng(Ind.Aerodyn) 1994; 51: 215-227.

[9] Mahaarachchi D, Mahendran M. Finite element analysis and design of crest-fixed trapezoidal steel claddings with wide pans subject to pull-through failures. Eng Struct 2004; 26 (11): 1547–1559.

[10] Mahaarachchi D, Mahendran M. Wind uplift strength of trapezoidal steel cladding with closely spaced ribs. J.Wind Eng(Ind.Aerodyn) 2009; 97: 140-150.

[11] Mahaarachchi D, Mahendran M. A strain criterion for pull-through failures in crest-fixed steel claddings. Eng Struct 2009; 31 (2): 498-506.

[12] Henderson D, Ginger J. Response of pierced fixed corrugated steel roofing systems subjected to wind loads. Eng Struct 2011; 33 (12): 3290-3298.

[13] Lovisa A, Henderson D, Ginger J. Characterising fatigue macrocrack initiation in profiled steel roof cladding. Eng Struct 2016; 125 (15): 364–373.

[14] ECS, EN 1993-1-3: Design of Steel Structures - Part 1–3: General Rules - Supplementary Rules for Cold-formed Members and Sheeting, European Committee for Standardization (ECS), Brussels, Belgium, 2006.
[15] American Iron and Steel Institute (AISI). North American Specification for the Design of Cold-formed Steel Structural Members, AISI S100-07; 2007.
[16] ISO E, 6892-1, Metallic Materials–Tensile Testing—Part 1: Method of Test at Room Temperature ISO E, 6892-1, International Standard, Geneva, 2009.
[17]Standards Australia. AS/NZS1170.2:2002 Structural design actions part 2: wind actions. AS/NZS11702:2002. Sydney (NSW, Australia): Standards Australia; 2002.
[18] Beck V, Stevens L. Wind loading failures of corrugated roof cladding. Civil Engineering Transactions IE Aust; 1979.
[19] Mahendran M, Mahaarachchi D. Splitting Failures in Trapezoidal Steel Roof Cladding. Journal of Performance of Constructed Facilities ASCE 2004; 18(1): 4-11.